Hindawi
Shock and Vibration
Volume 2021, Article ID 5089213, 16 pages
https://doi.org/10.1155/2021/5089213

Research Article

Design and Investigation of a Nonlinear Damper Based on Energy Dissipation through Shock and Dry Friction to Suppress Critical Self-Excited Vibrations in Drilling Systems

Vincent Kulke,[1] **Georg-Peter Ostermeyer**,[1] **and Andreas Hohl**[2]

[1]*TU Braunschweig, Institute of Dynamics and Vibrations, Braunschweig 38106, Germany*
[2]*Baker Hughes, Celle 29221, Germany*

Correspondence should be addressed to Georg-Peter Ostermeyer; gp.ostermeyer@tu-bs.de

Received 26 July 2021; Accepted 31 August 2021; Published 26 September 2021

Academic Editor: Peng Wang

In this paper, a passive damper based on energy dissipation through shock and dry friction (shock-friction damper) is investigated regarding its design and effectiveness for damping self-excited torsional vibrations similar to those occurring in deep drilling. The results are compared to the results of conventional friction dampers. The effectiveness of the damper for different operational drilling parameters that change during the drilling process, such as the weight on the bit and the rotary speed of the bit, is analyzed. Two linear reduced order models of a drill string that are based on a complex finite element model are set up. One is reduced using the component mode synthesis and one is reduced to the identified critical mode. A lumped mass represents the inertia of a forcedly connected nonlinear damper. A combined reduced order model of the complex system and the inertia damper is introduced to investigate its dynamic motion and stability. Particular focus is on the energy flow within the dynamic system and on the change of the dissipation energy in the contact. A semi-analytical solution is derived using the harmonic balance method that is used to investigate the damping effect for various designs and operational parameters. Herein, the modal properties as well as parameters of the damper are examined regarding the damping effect and the stability of the system. Finally, the capability of the mechanism to suppress the self-excitation due to the bit–rock interaction in a drilling system is discussed, and recommendations are made with respect to the design parameters and placement of the damper.

1. Introduction

In downhole drilling systems, various types of vibrations occur that can reduce drilling performance and reliability as well as increase premature failure of components and nonproductive time [1, 2]. Especially when drilling in hard and dense formations, high-frequency torsional oscillations (HFTO) occur [3] in a system-dependent frequency range between 50 Hz and 500 Hz. These oscillations are self-excited torsional vibrations of higher-order modes that are caused by the bit-rock interaction [4] and that can lead to critical torsional loads [1, 5]. Downhole measurement data show that in most cases one high-frequency torsional mode dominates the dynamic of the drilling system [6, 7]. The self-excitation mechanism, which leads to the critical torsional loads, can be modeled by a torque characteristic at the bit that is nonlinear with respect to the rotary speed (Figure 1) [8].

In [8], an analytical predictive criterion

$$S_{c,i} = \frac{-2D_i\omega_{0,i}}{\varphi_{i,\mathrm{bit}}^2} < \frac{d\mathrm{Torque}}{d\mathrm{RPM}}, \tag{1}$$

based on a modal transformation (modal damping constant D_i, natural angular frequency $\omega_{0,i}$, and deflection of the mass-normalized eigenvector of mode i at the bit $\varphi_{i,\mathrm{bit}}$) and linearization of the nonlinear torque characteristic at the bit (dTorque/dRPM) are introduced. This $S_{c,i}$ criterion is used to determine modes that are unstable and thus prone to self-excitation. Additionally, based on the observation that no backward rotation of the bit can occur [4], a criterion for the worst-case amplitude $\hat{x} = (2\pi/(60\mathrm{sec/min}))\mathrm{RPM}\,(1/\omega_{0,i})$ of

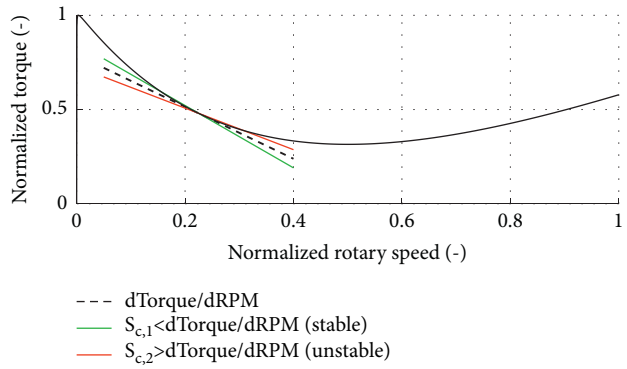

Figure 1: Nonlinear torque characteristic with lines at the operating point c.f. [9, 10].

these critical modes is derived [9]. The worst-case amplitude is a reliable criterion when one mode dominates the dynamic of the system, but also delivers good results if an interaction between low-frequency stick/slip and HFTO is observed [6]. In [10], this interaction is analyzed using downhole measurement data and simulations of a modal reduced order model representing the torsional mode of stick/slip and HFTO. The bit–rock interaction is modeled as a nonlinear drilling torque characteristic as a function of the rotary speed and weight on bit (WOB) similar to Figure 1. Through the resulting stability maps, suitable drilling conditions are determined by adjusting operational parameters such as rotary speed or WOB to reduce critical drill string vibrations based on the overlap of the stability maps of stick/slip and HFTO. Besides reducing the WOB that results in a smaller negative slope of the torque characteristic, an increase of the rotary speed can stabilize the system due to an increasing torque characteristic at high rotary speeds (Figure 1). Furthermore, the stable areas in the stability maps can be extended by adding damping to the system [11–13]. Since the drilling parameters cannot be adjusted arbitrarily, further concepts have to be investigated. In downhole drilling systems, concepts based on isolation [14], energy transfer [15], and additional damping [12, 13] have been discussed in the literature.

Additional tools that are placed within the drill string have been investigated to reduce critical torsional vibration. In [14], an isolator tool is investigated in simulation, laboratory tests, and operation. This tool, which is based on the principle of a mechanical low-pass filter, can isolate critical areas of the bottom-hole assembly (BHA) from torsional vibrations induced by the bit–rock interaction. Increasing the damping of a system is another well-known approach to reduce self-excited vibration amplitudes [16]. Tondl investigated the effect of tuned mass dampers [17] and dry friction [18] on self-excited vibrations. Some types of friction contacts and friction dampers for various fields of engineering were investigated and classified [19]. Examples for vibration reduction through friction damping are found in the field of gas turbines [20], mounted structures [19], and railway wheels [21, 22]. In the field of drilling systems, the effectiveness of inertia-based and stiffness-based dampers are analyzed in [12], and a nonlinear tuned damper is analyzed in [13]. Due to the small design space in the BHA that is naturally limited by the drilled borehole diameter, the additional damping provided by the damper is limited and possibly not sufficient to stabilize unstable self-excited vibrations.

Similar efforts for nonlinear attachments show a significant effect on the energy output and stability of dynamic systems [23, 24]. While the damping effect of friction is directly related to the dissipation processes in the contact, the energy transfer caused by shocks can have various effects on the dynamic motion and energy balance of the system. Shocks can add energy to a system, dissipate energy from the system, and redistribute energy within the system. In [25], shocks are used to suppress self-excited vibrations through energy transfer from low- to high-frequency modes, which results in an increased damping ratio. Another possibility to use shocks to reduce vibrations are various types of impact dampers. These dampers range from simple lumped masses coupled to a structure by a mechanical backlash [26, 27] up to self-tuning impact vibration dampers [28]. In general, an impact damper causes shocks as soon as a clearance width is exceeded. Due to the collision between the impact damper and a structure, energy is dissipated and momentum is exchanged between the impact damper and the structure. Various impact dampers have already been analyzed analytically [29] as well as in simulations and experiments [30].

The challenges in drill string dynamic and the possibility of influencing the energy balance and, if applicable, the damping effect through shocks necessitates further investigation. Optimization of these highly nonlinear damping concepts to increase the provided damping for critical torsional modes, hence stabilize the self-excited modes, is important. In the following article, a friction damper comparable to [12, 21] is combined with an impact damper through an additional mechanical backlash that results in shocks between the structure and the damper [31, 32]. The resulting shocks can increase the damping effect through energy transfer from the self-excited structure to the damper and thus increase the dissipated energy in the friction contact. The increase in damping is evaluated qualitatively and quantitatively, and the influences of critical parameters are investigated regarding the stability of self-excited drill string modes. A semi-analytical and an analytical solution for the design of the damper is derived by using the harmonic balance method. The semi-analytical solutions are compared to time domain simulations of an entire self-excited drilling system.

2. Modelling a Passive Shock-Friction Damper in a Drilling System

To investigate drill string vibrations, a finite element model of an entire drill string (Figure 2) with the vector of angular deviations x from the operating point (for a constant angular speed and twist) with $\mathbf{M}\ddot{\mathbf{x}} + \mathbf{C}\dot{\mathbf{x}} + \mathbf{K}\mathbf{x} = \mathbf{f}$ is used. Herein, $\mathbf{M}, \mathbf{C}$, and $\mathbf{K}$ are the mass, damping, and stiffness matrices, and $\mathbf{f}$ is an external force vector.

To perform an efficient and accurate investigation of the dynamic motion of various additional dampers like the

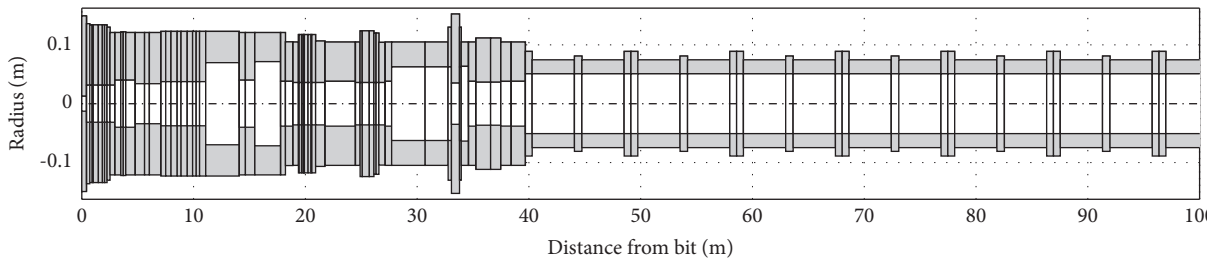

Figure 2: Model of a generic drill string.

nonlinear shock-friction damper, a reduced order model of the complex finite element model of the drilling system is derived.

In the following section, two reduction methods are carried out. First, the system is reduced using the component mode synthesis (CMS or Craig-Bampton method) resulting in a multiple-degree-of-freedom system with modal and physical degree-of-freedom [33, 34]. Second, the system is modally reduced to a modal single-degree-of-freedom system, representing the most critical and therefore dominant mode of the system [8, 12, 13]. Finally, a nonlinear damper is added to the different linear models of the drilling system. In both cases, the shock-friction damper is forcedly connected to the structure at one specific point of the BHA.

2.1. Component Mode Synthesis. The component mode synthesis is a reduction method based on a static and modal reduction, that is, specifically useful in systems with strong local nonlinearities to reduce the linear components [34]. All nodes u are divided into master u_{M} and slave u_{S} nodes and are rearranged regarding the mass M and stiffness matrix K according to

$$\begin{bmatrix} M_{\mathrm{SS}} & M_{\mathrm{SM}} \\ M_{\mathrm{MS}} & M_{\mathrm{MM}} \end{bmatrix} \begin{pmatrix} \ddot{u}_{\mathrm{S}} \\ \ddot{u}_{\mathrm{M}} \end{pmatrix} + \begin{bmatrix} K_{\mathrm{SS}} & K_{\mathrm{SM}} \\ K_{\mathrm{MS}} & K_{\mathrm{MM}} \end{bmatrix} \begin{pmatrix} u_{\mathrm{S}} \\ u_{\mathrm{M}} \end{pmatrix} = \begin{pmatrix} 0 \\ p_M \end{pmatrix}. \tag{2}$$

The master nodes are kept as physical coordinates where nonlinear forces act, while the slave nodes are modally reduced to so-called fixed interface modes. First, the static transformation matrix T_{stat} is determined $u_{\mathrm{S}} = K_{\mathrm{SS}}^{-1} K_{\mathrm{SM}} u_{\mathrm{M}} = T_{\mathrm{stat}} u_{\mathrm{M}}$. Second, the dynamic transformation matrix T_{dyn} is determined by a modal transformation of the slave nodes (with fixed master nodes) through $M_{\mathrm{SS}} \ddot{u}_{\mathrm{S}} + K_{\mathrm{SS}} u_{\mathrm{S}} = 0$, resulting in the transformation matrix T.

$$T = \begin{bmatrix} T_{\mathrm{dyn}} & T_{\mathrm{stat}} \\ 0 & E \end{bmatrix}, \tag{3}$$

with the uniform matrix E. The new transformed mass M_{T} and stiffness matrix K_{T} are calculated using

$$\begin{aligned} M_{\mathrm{T}} &= T^T M T, \\ K_{\mathrm{T}} &= T^T K T. \end{aligned} \tag{4}$$

The system is reduced by consideration of only a subset of modes in the modal transformation matrix, hence reducing the number of fixed interface modes [33] (rank of the matrix). As a thumb rule, all fixed interface modes with frequencies smaller than three times the characteristic frequency should be considered [35]. A convergence analysis has shown similar results in drill string dynamics. The CMS model used here has three master nodes, one master node at the bit $u_{\mathrm{M,bit}}$ (lowest node of the BHA model), where the nonlinear forces from the bit–rock interaction occur (Figure 1), one master node at the top drive $u_{\mathrm{M,top}}$ (highest node of the BHA model), where the constant rotary speed is applied and one master node $u_{\mathrm{M,d}}$ where the damper is connected to the BHA. The first two master nodes can be neglected when linearizing the motion of the BHA with respect to the operating point (average rotary speed and average torque at the bit).

The bit-rock interaction is modeled by a torque characteristic that is nonlinear with respect to the relative velocity between the bit and the rock (Figure 1). If the system is linearized to a specific operational rotary speed, the nonlinear torque characteristic with a negative/positive slope is equivalent to a negative/positive modal damping ratio [8]. Therefore, the self-excitation mechanism in the operational parameters can be modeled by a negative modal damping of the critical mode or modes.

2.2. Modal Reduction. Downhole measurement data show that in most cases when HFTO occur, one critical mode dominates the dynamic motion of the entire drill string [6, 7]. In this case, the dynamic motion of the entire drill string can be modeled by a modal single-degree-of-freedom system:

$$\ddot{q} + 2D_i\omega_{0,i}\dot{q} + \omega_{0,i}^2 q = \sum_{j=1}^{n} \varphi_{i,j} M_j, \tag{5}$$

where $\omega_{0,i}$ and D_i are the natural frequency and modal damping ratio of the ith mode q ($D_i < 0$ for self-excited modes). M_j is an external torque that acts on the jth node, and $\varphi_{i,j}$ is the mass-normalized modal amplitude of the ith mode shape at the jth node. In [8], a predictive criterion is derived through modal transformation and linearization of the rotary speed-dependent friction characteristic at the bit, resulting in $S_{\mathrm{c},i} = -2D_i\omega_{0,i}/\varphi_{i,\mathrm{bit}}^2$ for every mode. The self-excitation occurs due to the bit–rock interaction, hence $\varphi_{i,\mathrm{bit}}$ is the mass-normalized modal amplitude at the bit. Using this criterion, the dominant (most critical) mode is determined. This mode is considered as the ith and only mode in the minimal model.

2.3. Additional Friction-Based Damper. Any nonlinear torque can act at the master node $u_{\mathrm{M,d}}$ of the CMS reduced model or at any node (e.g., the jth node) of the minimal model with a mass-normalized amplitude of the mode shape $\varphi_{i,j}$. The added damper (Figure 3 (red)) consists of an inertia ring with a rotational inertia J. The torque between the inertia ring (Figure 3 (red)) and the structure (Figure 3 (blue)) consists of a friction contact with a normal force F_{N}, a coefficient of friction μ, and a friction radius r as well as a mechanical backlash with a contact stiffness c, damping constant d, an angular backlash width β_{S}, and a linearity constant e which models a linear stiffness and damping value for $e = 1$ and a nonlinear stiffness or damping value for $e \neq 1$ (e.g., Hertzian stiffness $e = 3/2$).

$$M\left(x_{\mathrm{rel}}, v_{\mathrm{rel}}\right) = \begin{cases} F_{\mathrm{N}}\mu r \operatorname{sgn}\left(v_{\mathrm{rel}}\right), & \left|\varphi_{i,j}q - x\right| < \beta_{\mathrm{S}}, \\ F_{\mathrm{N}}\mu r \operatorname{sgn}\left(v_{\mathrm{rel}}\right) + dv_{\mathrm{rel}}^{e} + c\left(\left|x_{\mathrm{rel}}\right| - \beta_{\mathrm{S}}\right)^{e} \operatorname{sgn}\left(x_{\mathrm{rel}}\right), & \left|\varphi_{i,j}q - x\right| \geq \beta_{\mathrm{S}}. \end{cases} \tag{6}$$

The relative angular speed v_{rel} and the relative angular displacement x_{rel} between the structure and the damper are $v_{\mathrm{rel}} = \varphi_{i,j}\dot{q} - \dot{x}$ and $x_{\mathrm{rel}} = \varphi_{i,j}q - x$ in the minimal model and $v_{\mathrm{rel}} = \dot{u}_{\mathrm{M,d}} - \dot{x}$ and $x_{\mathrm{rel}} = u_{\mathrm{M,d}} - x$ in the CMS reduced model. The equation of motion for the minimal model with a linear, nondissipating contact ($e = 1$ and $d = 0$) and a linearized torque characteristic at the bit that results in a negative modal damping ratio $D_i + D_{\mathrm{bit}} < 0$ is

$$\begin{pmatrix} 1 & 0 \\ 0 & J \end{pmatrix}\begin{pmatrix} \ddot{q} \\ \ddot{x} \end{pmatrix} + \begin{pmatrix} 2\left(D_i + D_{\mathrm{bit}}\right)\omega_{0,i} & 0 \\ 0 & 0 \end{pmatrix}\begin{pmatrix} \dot{q} \\ \dot{x} \end{pmatrix} + \begin{pmatrix} \omega_{0,i}^{2} & 0 \\ 0 & 0 \end{pmatrix}\begin{pmatrix} q \\ x \end{pmatrix} = \begin{pmatrix} -\varphi_{i,j}M\left(\varphi_{i,j}q - x, \varphi_{i,j}\dot{q} - \dot{x}\right) \\ M\left(\varphi_{i,j}q - x, \varphi_{i,j}\dot{q} - \dot{x}\right) \end{pmatrix}, \tag{7}$$

with a contact torque

$$M\left(q, x\right) = \begin{cases} F_{\mathrm{N}}\mu r \operatorname{sgn}\left(\varphi_{i,j}\dot{q} - \dot{x}\right), & \left|\varphi_{i,j}q - x\right| < \beta_{\mathrm{S}}, \\ F_{\mathrm{N}}\mu r \operatorname{sgn}\left(\varphi_{i,j}\dot{q} - \dot{x}\right) + c\left(\left|\varphi_{i,j}q - x\right| - \beta_{\mathrm{S}}\right)\operatorname{sgn}\left(\varphi_{i,j}q - x\right), & \left|\varphi_{i,j}q - x\right| \geq \beta_{\mathrm{S}}, \end{cases} \tag{8}$$

between the structure and the damper. In the following time domain simulations, the sign function is approximated by $\operatorname{sign}(x) \approx (2/\pi)a\tan((\pi/2)\kappa x)$, with $\kappa = 20000$ which corresponds to high slope values of the nonlinear torque characteristic at relative velocities near zero.

The presented torsional shock-friction damper, described mathematically in (7) and (8), is illustrated in Figure 3. Figure 3 shows the added torsional shock-friction damper (red), represented by a ring mass with a gap, and a section of the drill string (blue) that are connected via a friction contact. The damper can only move rotationally on the structure and is limited by a torsional stop of the structure located in the gap of the damper.

3. Investigation and Comparison of the Minimal and CMS Reduced Models

In the following section, the time domain results from the modal minimal model and the CMS reduced model are analyzed and compared. In particular, the reduction of the drill string from multiple-degree-of-freedom to a modal single-degree-of-freedom is analyzed regarding the qualitative and quantitative accuracy of the model. Similar to [12], the various states of dynamic motion between the damper and the structure are observed. These four stages are the sticking regime, the stick-slip (mixed) regime, the pure sliding regime, and the shock regime. In [12], the friction damper without backlash is analyzed, and the first three regimes are shown in detail. Figure 4 shows the angular velocity of the critical mode (modal coordinates) and the damper (physical coordinates) in the sliding regime, where no shocks occur. Only the friction torque acts between the structure and the damper. In this state, stable limit cycles occur when the additional damping provided by the damper exceeds the negative damping from the self-excitation.

In both cases, the exponential increase of the amplitude due to self-excitation is observable for low amplitudes. When the inertia moment exceeds the friction torque, the relative displacement occurs in the friction contact between the structure and the damper, resulting in dissipated energy and an increase of the damping. Figure 4 shows that the results from the CMS reduced and minimal models agree qualitatively and quantitatively. Hence, in this regime, the reduction to a single-degree-of-freedom is valid. Figure 5 shows the angular speed in the shock regime. Here, in both cases, the angular speed of the damper and the structure are

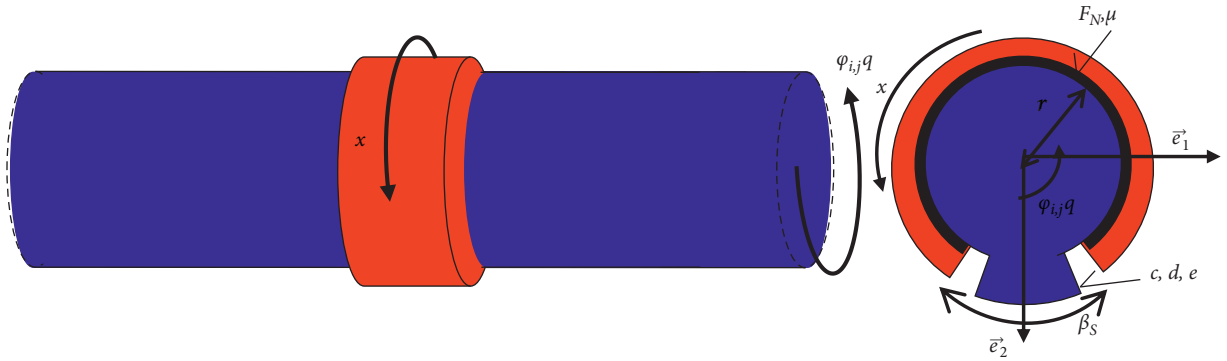

Figure 3: Principle sketch of a shock-friction damper in a drill string.

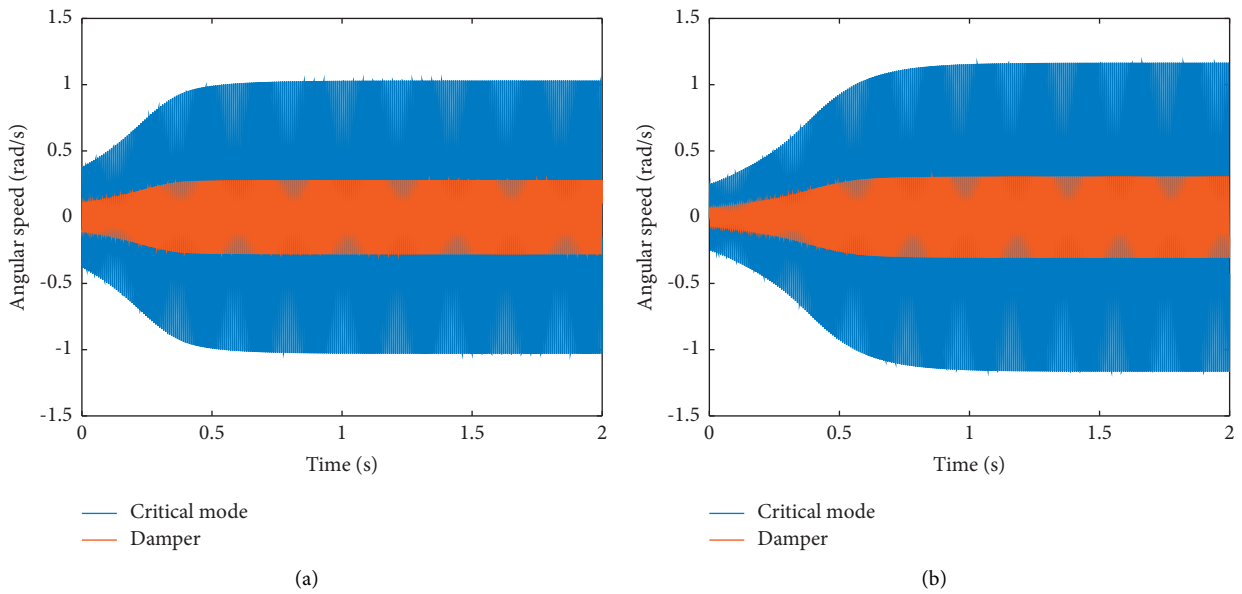

Figure 4: Time response of the damper (physical) and structure (modal) without shocks, using a CMS-reduced model (a) and a modal-reduced model (b).

shown in physical coordinates. The CMS reduced and the minimal model show, in contrast to Figure 4 and [12], the additional shock state. First, the amplitudes increase exponentially; then, a relative displacement occurs in the sticking and sliding (mixed regime) and the pure sliding regime, between the inertia damper and the contact point in the drilling system. If the additional damping provided by the damper is not sufficient to stabilize the system, the amplitudes related to the drilling system further increases. Hence, the amplitude of the structure further increases but, due to the additional damping, at a lower rate. Finally, the shock phase occurs where the relative angular displacement between the damper and the structure is higher than the backlash width. The resulting shocks can lead to high damping ratios and therefore a reduction of the amplitude of the critical mode. Subsequently, the phases repeat again.

Especially in the shock phase, the energy transferred between various modes of the CMS reduced model gives significant information about the importance of the other modes in the multiple-degree-of-freedom system. Figure 6 shows the modal energy of the five modes with the highest modal energy. A common phenomenon in drill string dynamics is that only one higher-order mode is unstable (self-excited). In the analyzed system, the fifth mode is self-excited. In Figure 6, the various phases are easily identified in the modal energy. First, an exponential increase of the modal energy (1) is observed. At some point, the additional damping from the damper reduces but does not stop the increase of the modal energy (2). The amplitude increases further, which leads to shocks (3). The shocks are shown in the modal energy by a sudden decrease of the modal energy of the critical mode (fifth mode). The other modes show a slight increase in the modal energy. Nevertheless, due to the small positive modal damping ratio and the high frequency of the other modes, the transferred modal energy is quickly dissipated, hence negligible.

These results show two major aspects. First, the nonlinear damper does influence other modes of the structure, especially in the shock phase, but these influences can be neglected here. In this case, the reason for the negligible

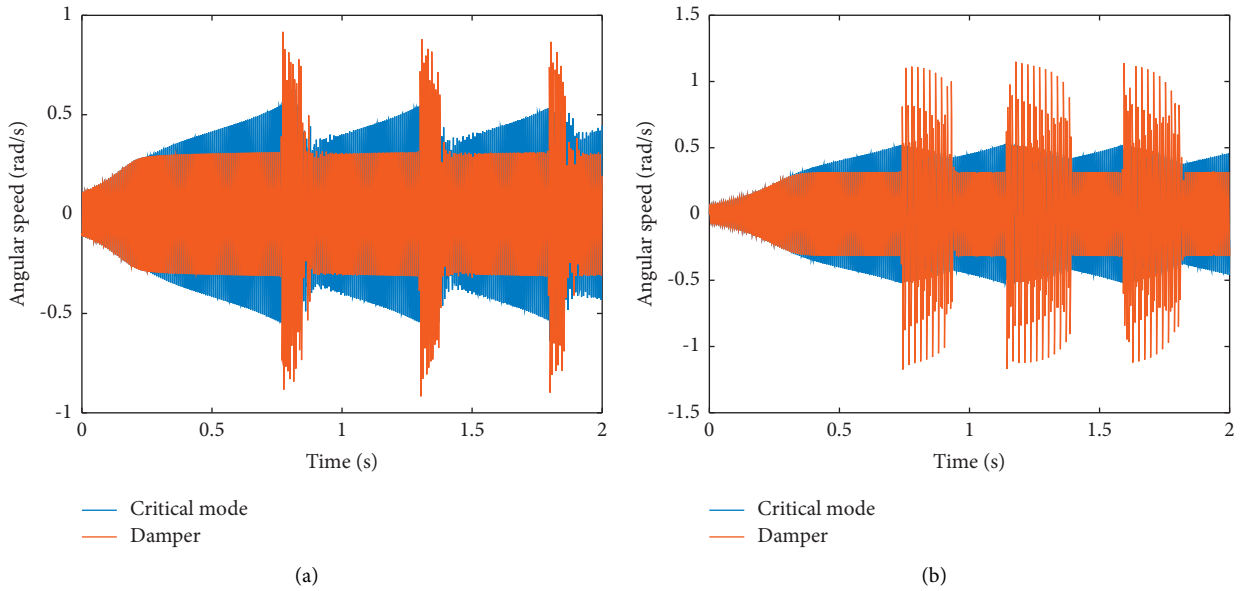

Figure 5: Time response of the damper (physical) and structure (physical amplitude at the damper) with shocks, using a CMS-reduced model (a) and a modal-reduced model (b).

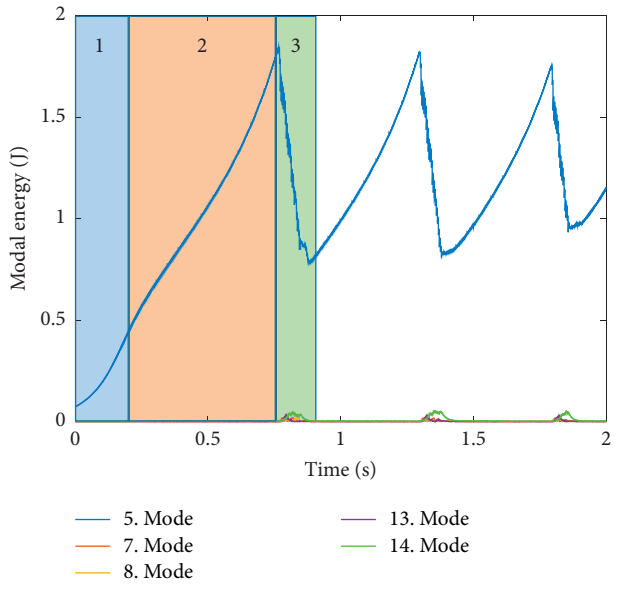

Figure 6: Modal energies of the five modes with the highest modal energy in the shock phase.

response of the other modes is a small mass-normalized eigenvector of the drill string modes at the damper location that directly influences the transfer of the shock to these modes. Second, the small quantitative differences between the two models can be attributed to the higher reactive effect of the damper on the overall dynamics of the structure in the minimal model. The response is highly dependent on the inertia of the connected damper and can lead to, e.g., a frequency-related detuning of the system, especially in the minimal model. As the diameter of the damper is limited through the borehole and tool diameter of the drilling system, only relatively small rotational inertia can be realized. This leads to a negligible effect of the damper on the dynamics (e.g., mode shape, natural frequency) of the system. In the following section, primarily the shock phase of the minimal model is examined in time domain.

4. Analysis of the Vibration Response and Energy Flow in Time Domain

By adjusting the parameters, all phases of the relative displacement can be observed. Figure 7(a) shows the angular speed of the structure and the damper in time domain derived with the minimal model similar to Figure 5. For small amplitudes, sticking occurs in the frictional contact between the damper and the drilling system and no relative movement between the structure and the damper can be observed. Due to the self-excitation ($D_i < 0$), energy periodically accumulates in the system (Figure 7(b)), resulting in an increase of the amplitude of the structure in the sticking phase. At a certain amplitude of the structure, the inertial torque of the damper is greater than the friction torque, $J\ddot{x} > F_N \mu r$, resulting in a relative displacement between the structure and the damper in the sliding regime, hence the energy dissipation in the friction contact. When the dissipated energy in the friction contact is not sufficient to stabilize the system, the amplitude further increases, which results in an increased relative displacement. When the relative displacement between the damper and the structure exceeds the backlash width, shocks occur between the damper and the structure.

These shocks, which do not occur in a conventional friction damper, lead to an energy transfer between the damper and the structure. Figure 7(b) shows that when a shock occurs, the energy is dissipated in the self-excited structure while the kinetic energy of the damper increases. This leads to two positive effects on the stability and energy

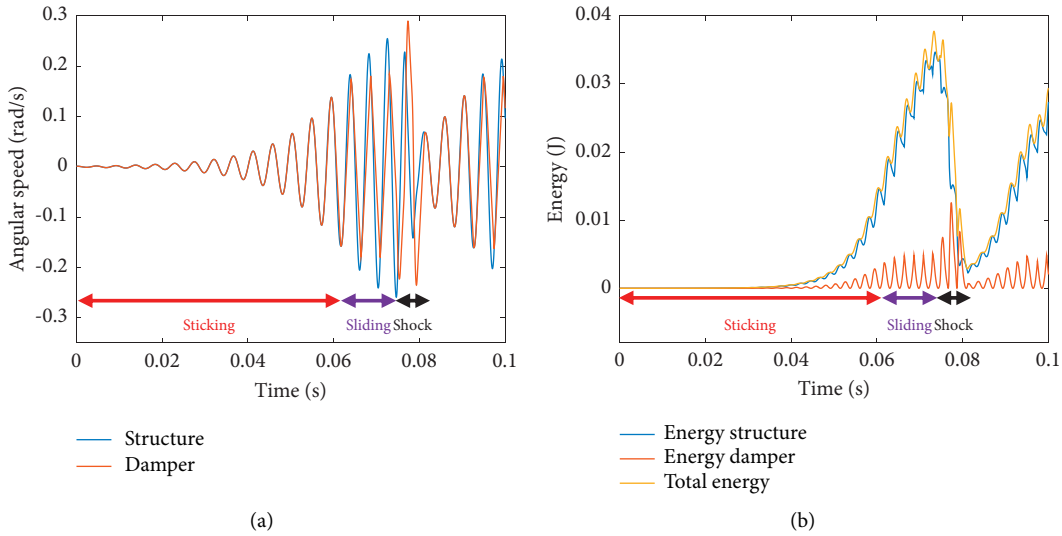

FIGURE 7: Time response of the damper and the structure (a); energy flow within the system (b).

output of the system. First, the energy transfer reduces the energy of the structure, resulting in a reduced amplitude and thus lower energy input due to self-excitation. Second, the energy transferred to the damper increases the relative angular speed between the damper and the structure, hence resulting in more energy dissipation in the friction contact. The first effect is rather indirect, as no energy is dissipated, but the energy flow into the system due to the self-excitation is reduced. The second effect is a direct dissipation through the friction contact between the structure and the damper. In this particular case with ($e = 1$ and $d = 0$), energy dissipation does not occur directly in the shock contact. To get a deeper understanding as well as to enable effective design and optimization strategies for the damper, the increased energy dissipation and damping related to the second effect are determined semi-analytically by using the harmonic balance method [36–38], hence assuming a constant harmonic motion of the structure.

5. Derivation of a Semi-Analytical Solution

Similar to [12], a semi-analytical solution for the shock-friction damper is derived from the minimal model by using the harmonic balancing method. To derive the semi-analytical solution from the minimal model, assumptions are made. The assumptions on which the minimal model is based are considered: one critical mode dominates the system dynamics at a time (shown in downhole data [6, 7]), the effect of the damper on the modal parameters of the structure is negligible (limited installation space [12]), and other modes are not excited due to friction or shock (no significant energy transfer Figure 6). It is further assumed that the influence of the damper torque on the dynamic movement of the structure is small and the oscillation of the structure is harmonic. In the friction regime where only friction occurs (Figure 4), a nearly harmonic motion with a constant amplitude can be observed in the time domain simulations. In contrast, Figures 5 and 7 show a transient response with strong changes in the amplitude due to the shocks. In the shock regime, the results from the semi-analytical solution have to be evaluated carefully. According to the harmonic balance method, the motion of the self-excited structure and its time derivations is modeled by

$$\begin{aligned} q &= \hat{q}\sin\left(\omega_{0,i}t\right), \\ \dot{q} &= \hat{q}\omega_{0,i}\cos\left(\omega_{0,i}t\right), \\ \ddot{q} &= -\hat{q}\omega_{0,i}^2\sin\left(\omega_{0,i}t\right), \end{aligned} \tag{9}$$

where $\hat{q}$ denotes the modal amplitude of the considered critical mode. For $|\varphi_{i,j}\hat{q}\sin(\omega_{0,i}t) - x| < \beta_S$, the relative displacement between the damper and the structure is smaller than the backlash angle β_S which results in the equation of motion

$$J\ddot{x} = F_N\mu r\,\mathrm{sgn}\left(\varphi_{i,j}\hat{q}\omega_{0,i}\cos\left(\omega_{0,i}t\right) - \dot{x}\right). \tag{10}$$

If $|\varphi_{i,j}\hat{q}\sin(\omega_{0,i}t) - x| \geq \beta_S$, the relative displacement is higher than the backlash, resulting in the equation of motion

$$J\ddot{x} = F_N\mu r\,\mathrm{sgn}\left(\varphi_{i,j}\hat{q}\omega_{0,i}\cos\left(\omega_{0,i}t\right) - \dot{x}\right) + c\left(\left|\varphi_{i,j}\hat{q}\sin\left(\omega_{0,i}t\right) - x\right| - \beta_S\right)\mathrm{sgn}\left(\varphi_{i,j}\hat{q}\sin\left(\omega_{0,i}t\right) - x\right). \tag{11}$$

Using (10) and (11), the steady-state motion of the damper x and the torque $M(q, x)$ between the damper and the structure are determined semi-analytically (by approximating the sgn function) or by sectional linearization

(Appendix). With this information, the equivalent damping of the damper on the structure is determined by averaging the dissipated energy E_d over one period. Following the averaging of the dissipated energy, the equivalent damping D_{eq} is determined by transferring the dissipated energy E_d from the nonlinear contact to a linear modal damping. For a harmonic motion of the mode representing the structure, the damping ratio D_{eq} is further simplified

$$D_{eq} = \frac{E_d}{2\omega_{0,i}\int_0^T \dot{q}^2 dt} = \frac{E_d}{2\pi\omega_{0,i}^2 \dot{q}^2}. \quad (12)$$

In [12], this method is used to derive an analytical and semi-analytical solution for a friction damper without shocks (equation (10)). Figure 8 shows a damping diagram for a friction damper (adjusted/normalized to 1% maximum damping). The analytical solution for the maximum equivalent damping $D_{eq,max} = (2/\pi^2)\varphi_{i,j}^2 J$, the amplitude where this maximum damping occurs $\hat{q}_{max} = (\pi F_N \mu r/\sqrt{2}\varphi_{i,j} J\omega_{0,i}^2)$, and the amplitude from which on sliding occurs $\hat{q}_{slid} = (F_N \mu r/\varphi_{i,j} J\omega_{0,i}^2)$ can be determined from the analytic results. These equations can be used to optimize the design of one or multiple friction dampers regarding various parameters, e.g., the provided damping, the effective amplitude range, and the positioning. Despite the analytical solutions, the dynamic motion in the mixed regime is determined semi-analytically.

Similar to Figure 8, a damping diagram for the shock-friction damper is determined as shown in Figure 9. In addition to the states of the friction damper without backlash (sticking-only, mixed, and sliding-only), Figure 9 shows the shock state. In the shock state, the additional damping provided by the damper is increased. The sudden increase of the damping corresponds to the increased dissipated energy in the friction contact due to the increased relative velocity due to the increase in kinetic energy shown in Figure 7(b).

Figure 9 shows that prior to the shock regime, both the friction and the shock-friction damper exhibit the same dynamic response. This is the case because when the modal amplitude of the underlying structure is small, the backlash width is not exceeded by the relative motion between the damper and the structure, i.e., no shocks occur.

6. Design and Parameter Sensitivity

One important design parameter of the shock-friction damper is the backlash width. The size of the backlash width determines the amplitude at which shocks and thus the energy transfer between the damper and the structure occur. Figure 10 shows the damping effect of the shock-friction damper for a specific design with variations of the backlash width.

The backlash limits the relative movement between the damper and the underlying structure. In the sticking regime, neither friction damping nor shocks occur. When the amplitude increases, this leads to relative motion between the structure and the damper, resulting in sliding

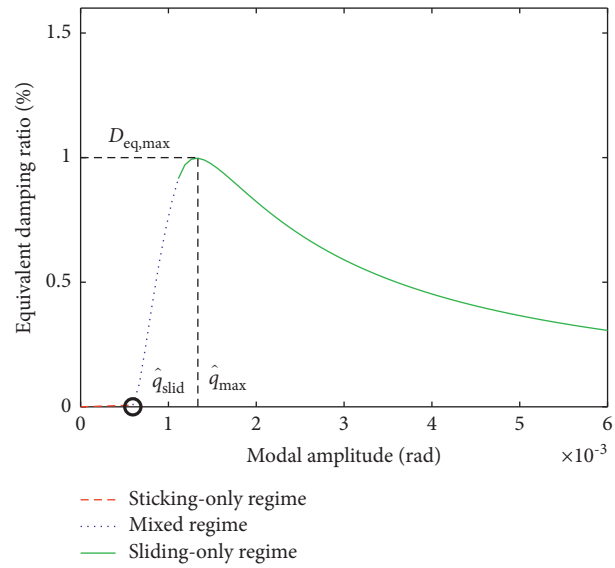

Figure 8: Semi-analytically determined damping diagram for a friction damper c.f. [12].

and thus an increased damping. Without the backlash, this leads to the underlying friction damping related curve (Figure 10 (black curve)). The additional shock damping is effective if the relative motion between the inertia damper and the structure exceeds the backlash width. The additional damping through the shocks with the mechanism described above is leading to a discontinuous damping curve in the transition from sliding friction to sliding friction with shocks. The amplitude of this discontinuity depends on the backlash width as observed in Figure 10. When the mechanical backlash width is too small, the movement of the damper is limited by the backlash. This limits the relative motion, resulting in a reduction of the dissipated energy and damping. For large backlash widths, the energy transfer from the structure to the damper due to the shocks occurs at high amplitudes. Although this results in a higher dissipated energy, the occurring higher amplitudes correspond to a lower damping ratio. The reason is that the damping is a ration between the dissipated energy and the corresponding amplitude. The optimal backlash width corresponds to the relative displacement amplitude near the maximum damping ratio of the friction damper (Figure 10 (black curve)). Near this amplitude, the proportion of the relative displacement, the friction torque, and the amplitude of the structure is leading to high equivalent modal damping ratios. To determine the optimum backlash width, an analytical equation for the rough design of the backlash width (angle β_s) of the shock-friction damper is derived. The maximum damping of the friction damper without backlash is in the sliding-only regime (Figure 8 and [12]). Here, the relative displacement $x_{rel} = x(t) - \varphi_{i,j}\hat{q}\sin(\omega t_1)$ can be solved analytically. In [12], the relative velocity in the sliding-only regime was solved analytically. To determine the relative

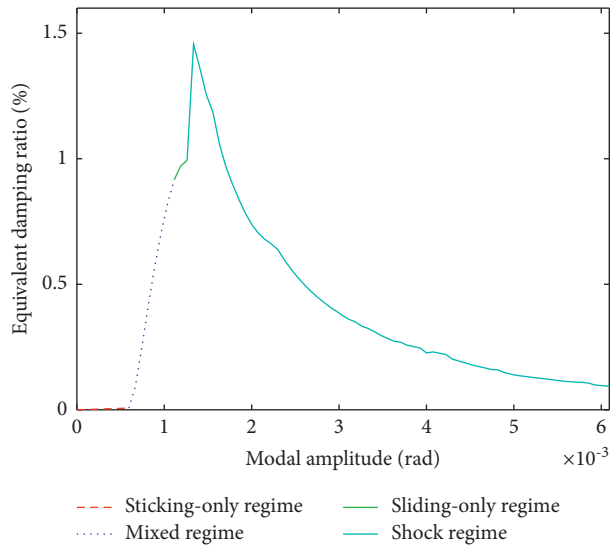

Figure 9: Semi-analytic determined damping diagram for a shock-friction damper.

displacement over half a period $(\pi/\omega_{0,i})$, the analytical solution for the relative velocity is

$$v_{\mathrm{rel}} = \pm \frac{F_{\mathrm{N}}\mu r}{J}\left(t - t_1\right) + \varphi_{i,j}\omega_{0,i}\widehat{q}\cos\left(\omega_{0,i}t_1\right) - \varphi_{i,j}\widehat{q}\omega_{0,i}\cos\left(\omega_{0,i}t\right), \tag{13}$$

and the time

$$t_1 = \frac{\arccos\left(\left(\pi F_{\mathrm{N}}\mu r/2J\widehat{q}\varphi_{i,j}\omega_{0,i}^2\right)\right)}{\omega_{0,i}}, \tag{14}$$

where the friction torque $F_{\mathrm{N}}\mu r$ changes the sign are integrated over half a period. Thus, the total distance traveled over half a period of pure sliding is determined. At the physical amplitude of the maximum damping of the friction damper without shock $\varphi_{i,j}\widehat{q}_{\max}$ (Figure 9), shocks should occur for optimal utilization of the backlash. This means that the total relative displacement at this amplitude should be equal to the total backlash angle $2\beta_{\mathrm{S}}$. Thus, via

$$\int_{t_1}^{t_1+\left(\pi/\omega_{0,i}\right)} v_{\mathrm{rel}}\left(\widehat{q}_{\mathrm{opt}}, t\right)\mathrm{d}t = \int_{t_1}^{t_1+\left(\pi/\omega_{0,i}\right)} -\frac{F_{\mathrm{N}}\mu r}{J}\left(t - t_1\right) + \varphi_{i,j}\omega_{0,i}\frac{\pi F_{\mathrm{N}}\mu r}{\sqrt{2}\varphi_{i,j}J\omega_{0,i}^2}\cos\left(\omega_{0,i}t_1\right) - \varphi_{i,j}\frac{\pi F_{\mathrm{N}}\mu r}{\sqrt{2}\varphi_{i,j}J\omega_{0,i}^2}\omega_{0,i}\cos\left(\omega_{0,i}t\right)\mathrm{d}t = 2\beta_{\mathrm{S}}, \tag{15}$$

the backlash angle (backlash width)

$$\beta_{\mathrm{S}} = \frac{F_{\mathrm{N}}\mu r\pi}{2J\omega^2}, \tag{16}$$

is determined. The other parameters like the inertia of the damper mass or positioning of the damper (mass-normalized modal amplitude at the friction contact) have a similar influence on the damping effect of the shock-friction damper as for the friction damper. Thus, both a higher damper inertia and especially a better positioning (higher mass-normalized modal amplitude) increase the damping effect. Similar results are shown in Figure 11. Similar to the conventional friction damper the friction torque, the coefficient of friction, the friction radius and the normal force do not influence the equivalent damping for an optimized backlash (equation (16)). The friction torque only scales the amplitude where the damping maximum occurs.

Unlike for the friction damper, the frequency has an influence on the damping effect of the shock-friction damper. Figure 12 shows the influence of the natural frequency of the underlying structure on the damping effect of the damper for a design where the backlash width is adjusted according to equation (16).

Figure 12 shows that the damping effect increases with an increasing frequency. This effect corresponds to a change in the stiffness c of the mechanical backlash contact. The stiffness and the natural frequency of the structure can be tuned. The optimum can be attributed to the absorber frequency $\omega_{0,i} \approx \sqrt{c/J}$. With this information, a rough

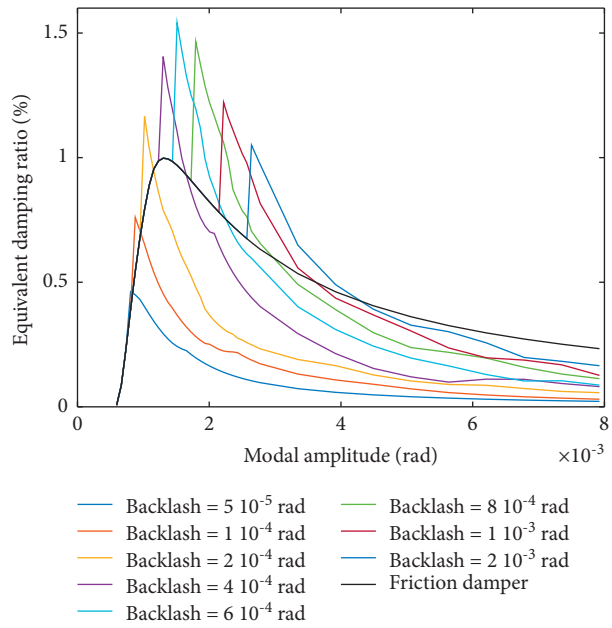

Figure 10: Influence of the mechanical backlash on the damping effect of the shock-friction damper.

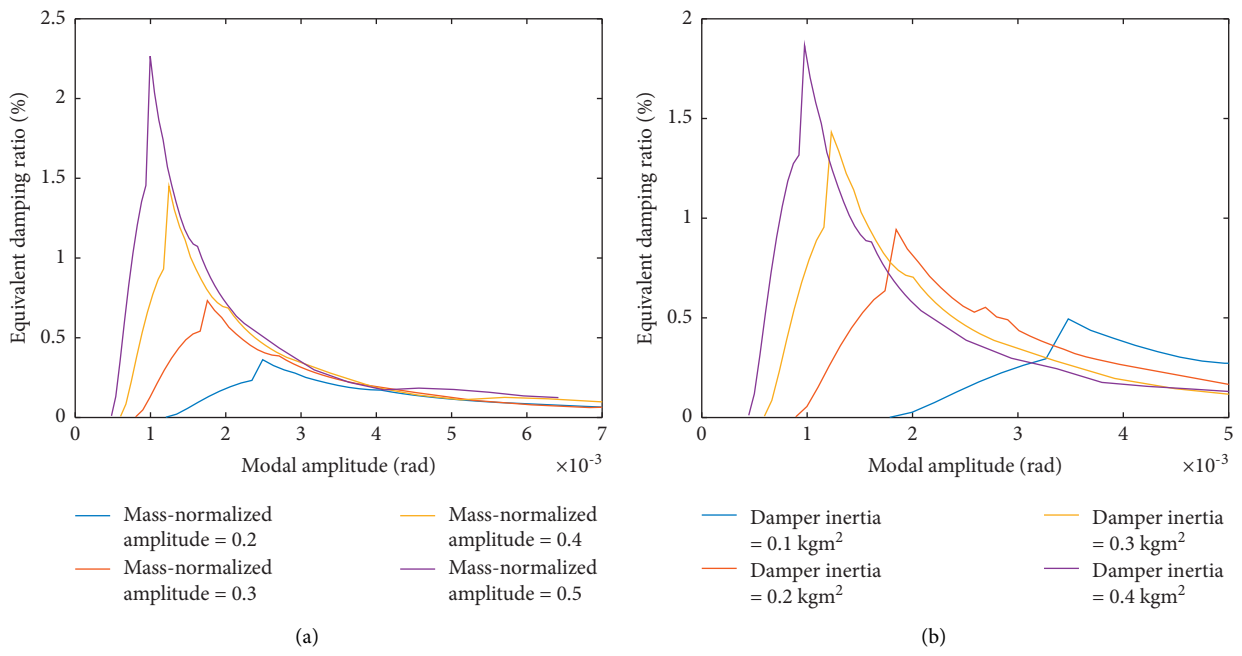

Figure 11: Influence of the mass-normalized modal amplitude at the damper (a) and the rotational inertia of the damper (b) on the equivalent damping ratio.

design of the damper is created. In highly nonlinear systems, the initial values have an influence on the system dynamic. Due to the mechanical backlash, the position of the damper relative to the structure is decisive. Depending on the position, shocks can occur even at very small amplitudes. The equations (Appendix) show that each shock causes a change in the angular speed of the damper. This can lead to a new solution of the steady state due to a change of the initial values. Figure 13 shows the damping effect of the shock-friction damper for two different initial conditions. The initial relative displacements between the structure and the damper are different. The initial condition where the damper is closer to one side of the mechanical backlash shows higher damping ratios at lower modal amplitudes. This is the case because at small amplitudes no shocks occur between the damper and the structure but due to the smaller initial relative displacements between the damper and the backlash, the shocks occur at smaller amplitudes. Although the friction torque would not be sufficient to surpass the backlash width, a

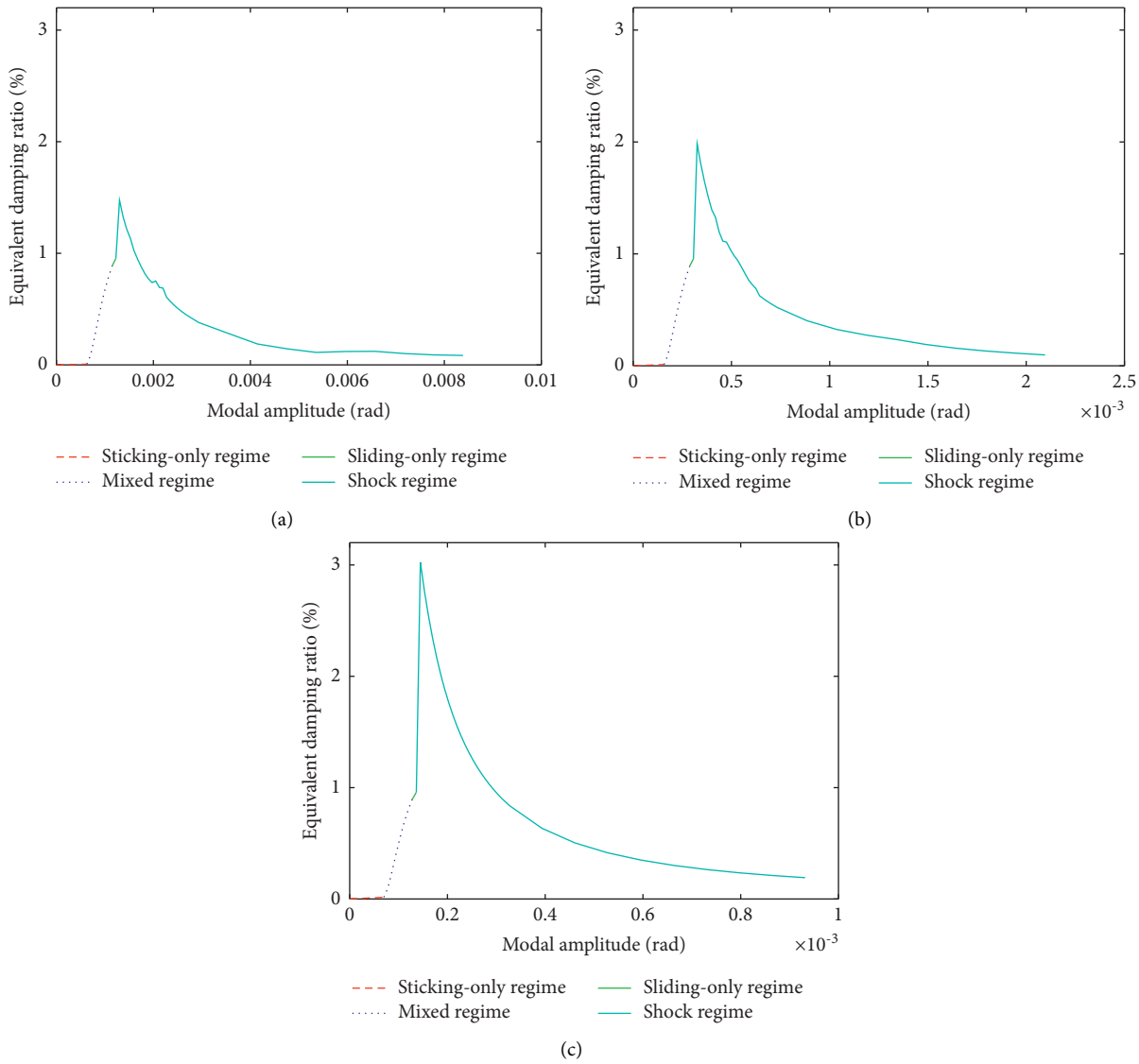

Figure 12: Influence of the natural frequency of the structure on the damping effect of the shock-friction damper (a) $f = 130$ Hz, (b) $f = 260$ Hz, and (c) $f = 390$ Hz with optimized backlash width.

steady state is reached because the shock itself increases the angular speed of the damper mass and thus the backlash width can be surpassed.

This can influence the damping effect and design of the damper. Therefore, the rough design using (16) should be improved by using the semi-analytical solution and, if necessary, extended by considering the uncertainties regarding the initial conditions as well as finally transferring the damper to self-excited systems. Figure 14 shows four different solutions for various amplitudes of the underlying structure, from simple T-periodic solutions with and without shocks (Figures 14(a) and 14(b)) to multiple nT-periodic solutions (Figure 14(c)) up to not periodic solutions (Figure 14(d)). The initial conditions have no influence on the equivalent damping when no shocks occur (Figure 14(a)).

Figure 14 shows the complexity of the dynamic motion, especially in the shock regime, because all possible states can occur in one period (shock, sliding, and sticking). Only steady-state solutions similar to Figure 14(a) can occur in the self-excited system. The other solutions in Figure 14 arise at amplitudes higher than the amplitude of the maximal damping, hence in self-excited systems these solutions are not observed and would represent an unstable solution.

7. Transfer to Self-Excited Drill String Vibrations

In the following section, the damping diagram from the semi-analytical solution is related to self-excited systems. Figure 15 shows the damping diagram of a shock-friction damper. Additionally, in Figure 15, three cases of self-excitation are shown that are modeled and varied by the absolute value of linearized negative damping ratios. The absolute value of the two self-excited damping ratios ($D_i = -0.7\%$, $D_i = -1.2\%$) result in intersections between

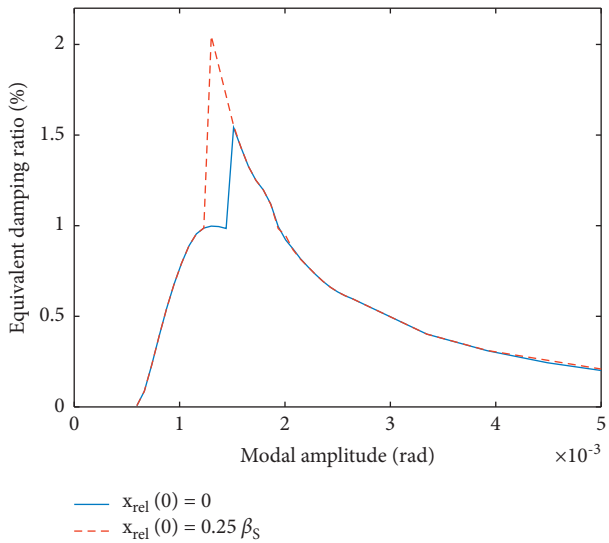

Figure 13: Influence of the initial values on the damping effect of the shock-friction damper.

the self-excitation and the damping provided by the damper. The absolute value of the third self-excitation ($D_i = -1.5\%$) is higher than the maximum damping provided by the damper and therefore no intersections occur.

Figure 16 shows the corresponding time domain results of the self-excited system. For all cases, an exponential increase for small amplitudes is shown that is corresponding to the sticking regime of a friction damper. For minor self-excitations (instability of $D_i = -0.7\,\%$), a steady state with a constant amplitude of the angular displacement of the structure is observed (Figure 16(a)), no shocks occur, and the damping effect related to friction is sufficient to stabilize the system. The stable limit cycle of Figure 16(a) is similar to the one with friction damping only in Figure 14(a). The amplitude of the angular displacement of the critical mode is similar to the modal amplitude at the intersection of the corresponding self-excitation with the provided damping in Figure 15, hence the damping diagram not only shows the provided damping but also the occurring amplitude of the limited cycle. When a system is self-excited, the amplitude increases until the energy balance is zero (dissipated energy $E_d = E_s$ self-excited energy) and a limited cycle occurs. In Figure 16(b), the energy input through self-excitation is increased to $D_i = -1.2\%$, resulting in a higher necessary damping to stabilize the system. The friction damping mechanism alone cannot provide sufficiently high additional damping to achieve a stable limit cycle with an acceptable amplitude. The additional shock phase increases the damping. This sudden increase of the damping leads to two major phases. First, for smaller amplitudes before the shocks occur, the self-excited energy E_s is higher than the dissipated energy in the friction contact E_d ($E_d < E_s$), leading to a positive energy balance and therefore an increase of the amplitude of the structure. At some point, the amplitude at which shocks occur is reached, and therefore, the additional damping provided by the damper is increased significantly. The sudden increase leads to an increase of the dissipated energy and thus a negative energy balance $E_d > E_s$. The rapid increase of the dissipated energy results in a sudden decrease of the amplitude of the structure. The decrease of the amplitude of the structure results in a decrease of the relative motion and thus an end of the shock phase and therefore a reduced additional damping. This means that, similar to the beginning, the energy input due to the self-excitation is larger than the damping provided by the damper ($E_d < E_s$). Therefore, the energy balance is positive, and the vibration amplitude of the structure increases until the shock range is reached again. In this context, the position of the damper relative to the structure is crucial. The new position can result in an increased or decreased damping ratio during the next shock phase. Therefore, the previously made considerations regarding the position of the damper relative to the structure are decisive (Figure 13), and the minimum damping ratio should be taken into account in the design.

Finally, the last case, the unstable case, is shown in Figure 16(c). Here the damping provided by the damper is neither in the friction nor in the shock phase sufficient to stabilize the unstable mode. For a linearized minimal model, this results in an exponential increase of the amplitude. In a real, not linearized system, a maximum amplitude is reached. In drill string dynamics, this maximum amplitude, which corresponds to the maximum limited cycle, is dependent on the average rotary speed ν_{RPM}(RPM, revolutions per minute) of the drill string. In [9, 11], an analytical solution for the maximum amplitude $\varphi_{i,bit}\widehat{q} = (2\pi\,\nu_{RPM}/60\;\omega_{0,i})$ was determined. These results show how the information of the semi-analytical solution can be transferred to the self-excited system.

Following this, any self-excited vibration with corresponding energy inputs lower than the maximum damping shown in Figure 15 is stabilized by the shock-friction damper. Due to the assumptions and approximations done to determine the semi-analytical solution and due to the small stable area at the maximum, this is not exactly the case. Self-excitation results in an increase of the amplitude. When this increase is higher than the stable area, the stabilizing effect of a damper can be undermined ("skipped"). The accuracy of the solution is highly dependent on the reactive effect of the damper on the modes of the structure. The reactive effect increases with the inertia J and mass-normalized amplitude at the point where the damper is connected to the structure $\varphi_{i,j}$. Due to the limited installation space in drilling systems that are naturally confined by the borehole size, the inertia J is rather small. Additionally, the mass-normalized amplitude of a drill string is, due to the high inertia of the structure, small. Hence, in general, the modal amplitude is two, three, or four times higher than the physical amplitude. This means that the excitability is low and thus the effects of the shocks on other modes are low. In the field of drill string dynamics, the semi-analytical results and the design equations are sufficiently accurate. The results can also be transferred to other dynamic systems where one mode dominates the system response and the reactive effect can be neglected.

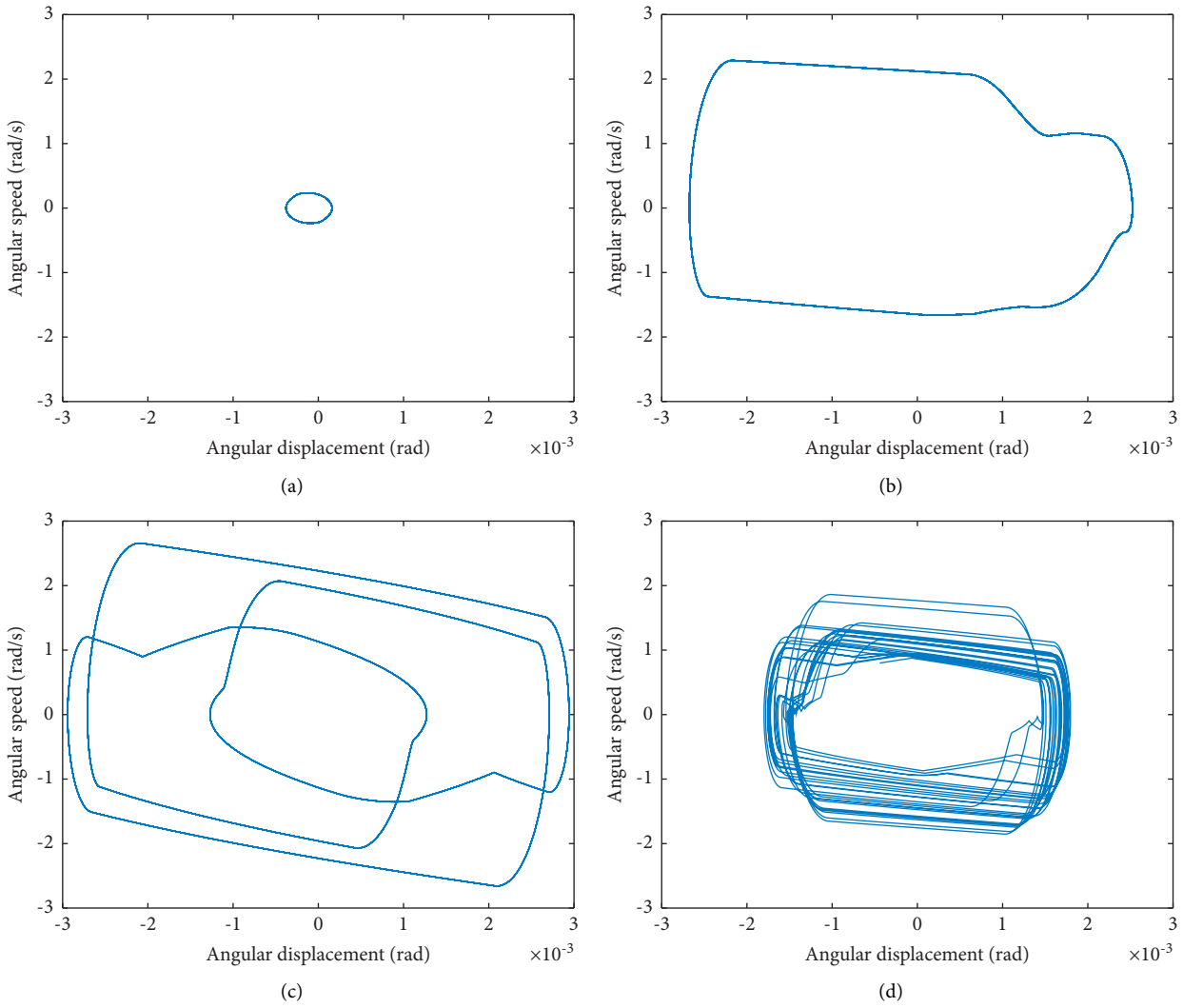

Figure 14: Phase space of the shock-friction damper for different steady-state solutions (various excitation amplitudes of the underlying structure) (a) limit cycle without shocks, (b) T-periodic limit cycle with shocks, (c) 3T-period, and (d) not periodic attractor.

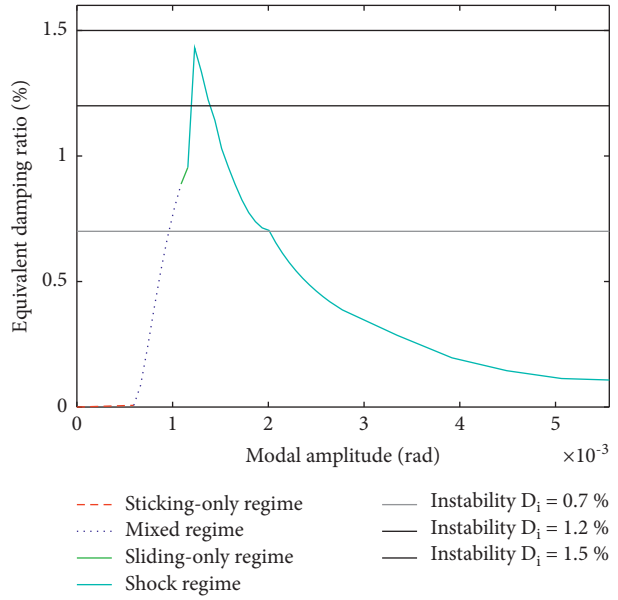

Figure 15: Semi-analytic determined damping diagram for a shock-friction damper with instabilities.

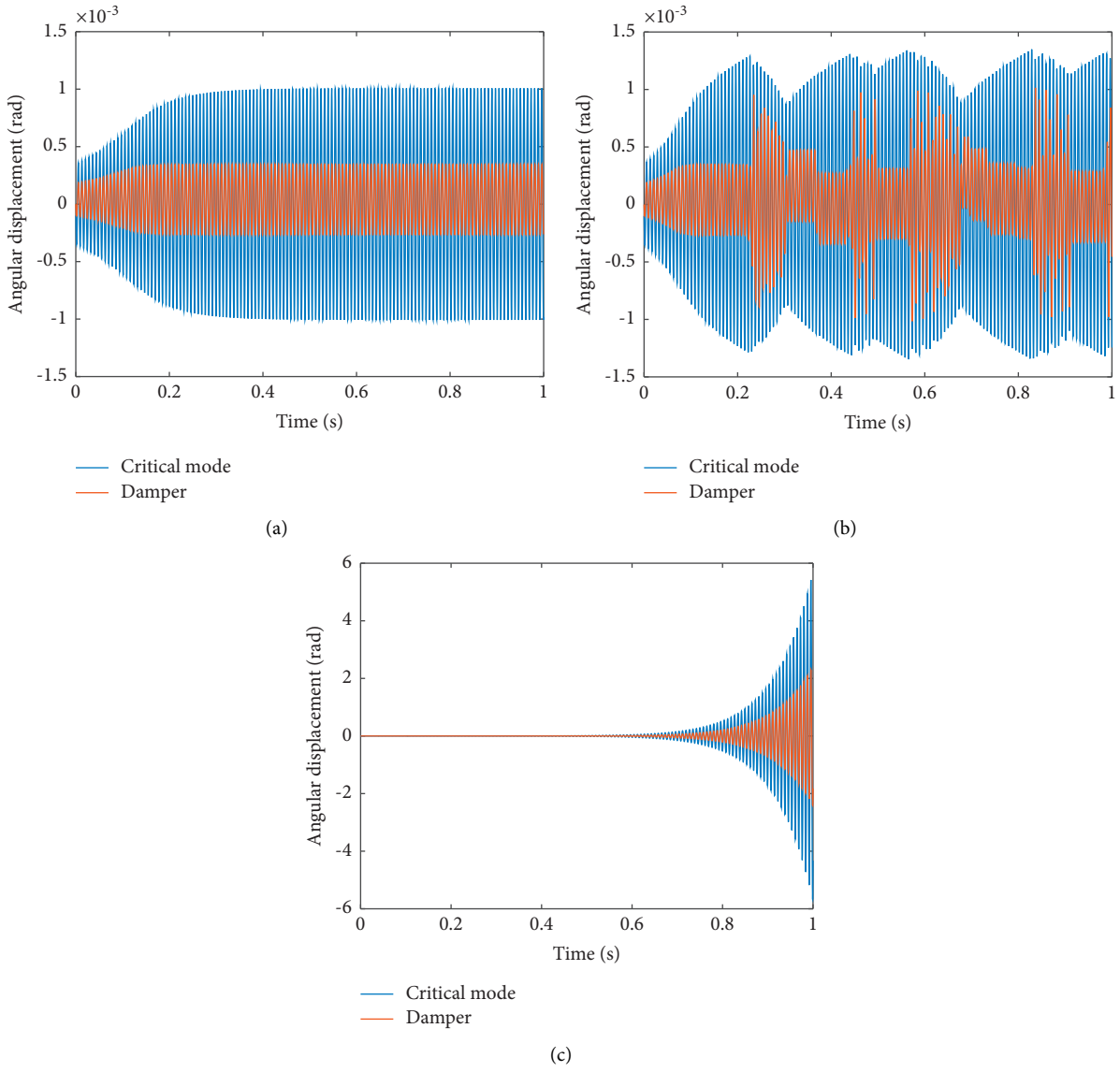

Figure 16: Time domain results from the self-excited minimal model for (a) $D_i = 0.7\%$, (b) $D_i = 1.2\%$, and (c) $D_i = 1.5\%$.

8. Conclusions

In this paper, a damper based on friction and shock is analyzed regarding its suitability to reduce self-excited HFTO in downhole drilling systems. A semi-analytical solution based on the harmonic balance is derived and compared with time domain simulations of a minimal model and an extended CMS reduced model. The semi-analytical solution is used to determine the damping that is provided by the damper for various parameters, e.g., the amplitude. This enables efficient optimization and design strategies regarding, e.g., position within the BHA, friction torque, and backlash width and reduces complex time domain simulations and stability analysis. An analytical equation to roughly design the backlash width of the nonlinear damper and influence its effective amplitude range is derived from the semi-analytical solution. Finally, the results are transferred to self-excited drill string vibration, and the characteristics are examined in detail, showing the accuracy and usability of the results. The combination of friction and backlash results in passive shocks, causing energy transfer between the self-excited structure and the damper that positively influences the energy output of the system. Compared to a conventional friction damper without backlash, an increase in the damping effect is achieved by adjusting the normal force and backlash width regarding the vibration frequency.

Appendix

Through sectional linearization, a semi-analytical solution is determined for the shock-friction damper. The seven different equations of motion consist of the sticking equation, two pure sliding equations, and four shock equations with various signs of the friction- and shock-torque. In the sliding regime for $|\varphi_{i,j}\widehat{q}\sin(\omega_{0,i}t) - x| < \beta_S$, the differential equation (equation (10))

$$J\ddot{x} = F_N \mu r \operatorname{sgn}\left(\varphi_{i,j}\hat{q}\omega_{0,i}\cos\left(\omega_{0,i}t\right) - \dot{x}\right), \tag{A.1}$$

is solved depending on the relative velocity by

$$\begin{aligned} x(t) \\ \dot{x}(t) &= \pm \frac{F_N \mu r}{J}\left(t - t_0\right) + \dot{x}\left(t_0\right), \\ \ddot{x}(t) &= \pm \frac{F_N \mu r}{J}. \end{aligned} \tag{A.2}$$

For the shock regime, hence $|\varphi_{i,j}\hat{q}\sin(\omega_{0,i}t) - x| \geq \beta_S$ the differential equation (equation (11))

$$J\ddot{x} = F_N \mu r \operatorname{sgn}\left(\varphi_{i,j}\hat{q}\omega_{0,i}\cos\left(\omega_{0,i}t\right) - \dot{x}\right) + c\left(\left|\varphi_{i,j}\hat{q}\sin\left(\omega_{0,i}t\right) - x\right| - \beta_S\right)\operatorname{sgn}\left(\varphi_{i,j}\hat{q}\sin\left(\omega_{0,i}t\right) - x\right), \tag{A.3}$$

is solved depending on the relative velocity and the relative displacement through $J\ddot{x} + cx = \pm F_N \mu r \pm \beta_S c + c\varphi_{i,j}\hat{q}\sin(\omega_{0,i}t)$ resulting in

$$\begin{aligned} x(t) &= \frac{\left(\pm F_N \mu r \pm \beta_S c\right)}{c} + \frac{c\varphi_{i,j}\hat{q}}{c - \omega^2 J}\sin\left(\omega\left(t - t_1\right)\right) + A\sin\left(\sqrt{\frac{c}{J}}\left(t - t_1\right)\right) + B\cos\left(\sqrt{\frac{c}{J}}\left(t - t_1\right)\right), \\ \dot{x}(t) &= \frac{c\varphi_{i,j}\hat{q}\omega}{c - \omega^2 J}\cos\left(\omega\left(t - t_1\right)\right) + A\sqrt{\frac{c}{J}}\cos\left(\sqrt{\frac{c}{J}}\left(t - t_1\right)\right) - B\sqrt{\frac{c}{J}}\sin\left(\sqrt{\frac{c}{J}}\left(t - t_1\right)\right), \end{aligned} \tag{A.4}$$

where A and B are determined by

$$\begin{aligned} A &= \frac{1}{\sqrt{c/J}}\left(\dot{x}\left(t_0\right) - \frac{c\varphi_{i,j}\hat{q}\omega}{c - \omega^2 J}\right), \\ B &= x\left(t_0\right) - \frac{\left(\pm F_N \mu r \pm \beta_S c\right)}{c}, \end{aligned} \tag{A.5}$$

and dependent on the initial condition $x(t_0)$ and $\dot{x}(t_0)$ at time t_0 were the new section starts. The final equation is the sticking equation where no relative velocity occurs, hence $\dot{x}(t) = \varphi_{i,j}\omega_{0,i}\hat{q}\cos(\omega_{0,i}t)$.

Data Availability

The data used to support the findings of this study are included within the article.

Conflicts of Interest

The authors declare that there are no conflicts of interest regarding the publication of this paper.

Acknowledgments

The authors would like to thank Baker Hughes for supporting the work and giving permission to publish this paper. We acknowledge support by the Open Access Publication Funds of the TU Braunschweig.

References

[1] H. Reckmann, P. Jogi, F. T. Kpetehoto, S. Chandrasekaran, and J. Macpherson, "MWD failure rates due to drilling dynamics," in *Proceedings of the IADC/SPE Drilling Conference and Exhibition*, New Orleans, Louisiana, USA, February 2010.

[2] A. I. Bowler, L. Logesparan, J. Sugiura, B. P. Jeffryes, R. J. Harmer, and M. Ignova, "Continuous high-frequency measurements of the drilling process provide new insights into drilling system response and transitions between vibration modes," in *Proceedings of the SPE Annual Technical Conference and Exhibition*, Amsterdam, The Netherlands, October 2014.

[3] H. Oueslati, J. R. Jain, H. Reckmann, L. W. Ledgerwood, R. Pessier, and S. Chandrasekaran, "New insights into drilling dynamics through high-frequency vibration measurement and modeling," in *Proceedings of the SPE Annual Technical Conference and Exhibition*, New Orleans, LA, USA, September 2013.

[4] J. R. Jain, H. Oueslati, A. Hohl et al., "High-frequency torsional dynamics of drilling systems: an analysis of the bit-system interaction," in *Proceedings of the IADC/SPE Drilling Conference and Exhibition*, Fort Worth, TX, USA, March 2014.

[5] H. Dennis, W. Mathäus, H. Christian, A. Hohl, and R. Hanno, "High-frequency torsional oscillation laboratory testing of an entire bottom hole assembly," in *Proceedings of the Abu Dhabi International Petroleum Exhibition & Conference*, Abu Dhabi, UAE, November 2017.

[6] A. Hohl, C. Herbig, P. Arevalo, H. Reckmann, and J. Macpherson, "Measurement of dynamics phenomena in

downhole tools–requirements, theory and interpretation," in *Proceedings of the IADC/SPE Drilling Conference and Exhibition*, Fort Worth, TX, USA, March 2018.

[7] H. Andreas, P. Eric, and A. Pedro, "Real-time system to calculate the maximum load of high-frequency torsional oscillations independent of sensor positioning," in *Proceedings of the SPE/IADC International Drilling Conference and Exhibition*, Hague, The Netherlands, 2019.

[8] A. Hohl, M. Tergeist, H. Oueslati et al., "Derivation and experimental validation of an analytical criterion for the identification of self-excited modes in drilling systems," *Journal of Sound and Vibration*, vol. 342, pp. 290–302, 2015.

[9] A. Hohl, M. Tergeist, H. Oueslati et al., "Prediction and mitigation of torsional vibrations in drilling systems," in *Proceedings of the IADC/SPE Drilling Conference and Exhibition*, Fort Worth, TX, USA, March 2016.

[10] A. Hohl, V. Kulke, A. Kueck, C. Herbig, G. Ostermeyer, and H. Reckmann, "The nature of the interaction between stick/slip and high-frequency torsional oscillations," in *Proceedings of the IADC/SPE International Drilling Conference and Exhibition*, Galveston, TX, USA, February 2020.

[11] A. Hohl, V. Kulke, A. Kueck et al., "Best practices for operations in HFTO prone applications," in *Proceedings of the SPE Asia Pacific Oil & Gas Conference and Exhibition*, Kuala Lumpur, Malaysia, November 2020.

[12] V. Kulke, G.-P. Ostermeyer, M. Tergeist, and A. Hohl, "Semi-analytical approach for derivation of an equivalent modal friction-damping ratio and its application in a self-excited drilling system," *Dynamics, Vibration, and Control*, vol. 4, 2019.

[13] V. Kulke, P. Thunich, F. Schiefer, and G.-P. Ostermeyer, "A Method for the design and optimization of nonlinear tuned damping concepts to mitigate self-excited drill string vibrations using multiple scales lindstedt-poincaré," *Applied Sciences*, vol. 11, no. 4, Article ID 1559, 2021.

[14] D. Heinisch, V. Kulke, V. Peters, C. Schepelmann, H. Reckmann, and G.-P. Ostermeyer, "Simulation and testing of an isolator tool for high-frequency torsional oscillation," in *Proceedings of the Abu Dhabi International Petroleum Exhibition & Conference*, November 2018.

[15] V. Kulke and G.-P. Ostermeyer, "Energy transfer through parametric excitation to reduce self-excited drill string vibrations," *Journal of Vibration and Control*, vol. 43, no. 1, 2021.

[16] A. Tondl, "To the problem of self-excited vibration suppression," *Engineering Mechanics*, vol. 15, no. 4, pp. 297–307, 2008.

[17] A. Tondl, "Quenching of self-excited vibrations equilibrium aspects," *Journal of Sound and Vibration*, vol. 42, no. 2, pp. 251–260, 1975.

[18] A. Tondl, "Quenching of self-excited vibrations: effect of dry friction," *Journal of Sound and Vibration*, vol. 45, no. 2, pp. 285–294, 1976.

[19] K. Popp, L. Panning, and W. Sextro, "Vibration damping by friction forces: theory and applications," *Journal of Vibration and Control*, vol. 9, no. 3-4, pp. 419–448, 2003.

[20] J. H. Griffin, "Friction damping of resonant stresses in gas turbine engine airfoils," *Journal of Engineering for Power*, vol. 102, no. 2, pp. 329–333, 1980.

[21] I. López, J. M. Busturia, and H. Nijmeijer, "Energy dissipation of a friction damper," *Journal of Sound and Vibration*, vol. 278, no. 3, pp. 539–561, 2004.

[22] I. Lopez and H. Nijmeijer, "Prediction and validation of the energy dissipation of a friction damper," *Journal of Sound and Vibration*, vol. 328, no. 4-5, pp. 396–410, 2009.

[23] A. F. Vakakis, L. A. Bergman, O. V. Gendelman, D. M. McFarland, G. Kerschen, and Y. S. Lee, *Nonlinear Targeted Energy Transfer in Mechanical and Structural Systems*, Springer Netherlands, Dordrecht, Netherlands, 2009.

[24] O. V. Gendelman, "Targeted energy transfer in systems with external and self-excitation," *Proceedings of the Institution of Mechanical Engineers - Part C: Journal of Mechanical Engineering Science*, vol. 225, no. 9, pp. 2007–2043, 2011.

[25] T. Pumhössel, "Suppressing self-excited vibrations of mechanical systems by impulsive force excitation," *Journal of Physics: Conference Series*, vol. 744, Article ID 12011, 2016.

[26] M. F. Dimentberg and D. V. Iourtchenko, "Random vibrations with impacts: a review," *Nonlinear Dynamics*, vol. 36, no. 2–4, pp. 229–254, 2004.

[27] S. Ema and E. Marui, "A fundamental study on impact dampers," *International Journal of Machine Tools and Manufacture*, vol. 34, no. 3, pp. 407–421, 1994.

[28] K. Duffy, R. Bagley, and O. Mehmed, "On a self-tuning impact vibration damper for rotating turbomachinery," in *Proceedings of the 36th AIAA/ASME/SAE/ASEE Joint Propulsion Conference and Exhibit*, p. 539, American Institute of Aeronautics and Astronautics, Reston, VA, USA, 2000.

[29] S. F. Masri and T. K. Caughey, "On the stability of the impact damper," *Journal of Applied Mechanics*, vol. 33, no. 3, pp. 586–592, 1966.

[30] J. Cheng and H. Xu, "Inner mass impact damper for attenuating structure vibration," *International Journal of Solids and Structures*, vol. 43, no. 17, pp. 5355–5369, 2006.

[31] B. Brogliato, *Nonsmooth Impact Mechanics: Models, Dynamics and Control*, Springer, Berlin, Germany, 1996.

[32] O. V. Gendelman and A. Alloni, "Forced system with vibro-impact energy sink: chaotic strongly modulated responses," *Procedia IUTAM*, vol. 19, pp. 53–64, 2016.

[33] R. R. Craig and M. C. C. Bampton, "Coupling of substructures for dynamic analyses," *AIAA Journal*, vol. 6, no. 7, pp. 1313–1319, 1968.

[34] J. Wijker, *Mechanical Vibrations in Spacecraft Design*, Springer, Berlin, Germany, 2004.

[35] M. A. d. Araújo Nunes and M. A. Viana Duarte, "Component mode synthesis method applied to two-dimensional acoustic analysis in ducts," *Journal of Vibration and Acoustics*, vol. 135, no. 1, p. 243, 2013.

[36] W.-J. Kim and N. C. Perkins, "Harmonic balance/Galerkin method for non-smooth dynamic systems," *Journal of Sound and Vibration*, vol. 261, no. 2, pp. 213–224, 2003.

[37] M. Krack and J. Gross, *Harmonic Balance for Nonlinear Vibration Problems*, Springer International Publishing, Cham, 2019.

[38] M. Nakhla and J. Vlach, "A piecewise harmonic balance technique for determination of periodic response of nonlinear systems," *IEEE Transactions on Circuits and Systems*, vol. 23, no. 2, pp. 85–91, 1976.